Icarus 216 (2011) 169–172

Contents lists available at SciVerse ScienceDirect

Icarus

journal homepage: www.elsevier.com/locate/icarus

Note

Regarding the possible generation of a lunar nightside exo-ionosphere

W.M. Farrell [a,d,*], J.S. Halekas [b,d], T.J. Stubbs [a,c,d], G.T. Delory [b,d], R.M. Killen [a,d], R.E. Hartle [a,b], M.R. Collier [a,d]

[a] NASA Goddard Space Flight Center, Code 695, Greenbelt, MD 20771, United States
[b] Space Science Laboratory, University of California at Berkeley, 7 Gauss Way, Berkeley, CA 94720, United States
[c] University of Maryland/Baltimore County, 1000 Hilltop Circle, Baltimore, MD 21250, United States
[d] NASA's Lunar Science Institute, Ames Research Center, Moffett Field, CA 94035, United States

ARTICLE INFO

Article history:
Received 23 May 2011
Revised 7 August 2011
Accepted 16 August 2011
Available online 24 August 2011

Keywords:
Moon
Ionospheres

ABSTRACT

The non-condensing neutral helium exosphere is at its most concentrated levels on the cold lunar nightside. We show herein that these He atoms are susceptible to impact ionization from primary and secondary electrons flowing in the vicinity of the negatively-charged nightside lunar surface. The secondary electron beams are a relatively recent discovery and are found to be emitted from the nightside surface at energies consistent with the negative surface potential. The effect is to create an electron impact-created ionosphere in nightside regions, possibly especially potent within polar craters.

Published by Elsevier Inc.

1. Introduction

The Moon possesses a tenuous surface bounded exosphere consisting primarily of argon and helium atoms, but also traces of sodium, potassium and possibly radon (see review by Stern (1999)). On the lunar dayside a fraction of these exospheric species becomes photo-ionized to create an 'exo-ionosphere' that has been directly detected by surface packages (see Collier et al. (2011) and references therein) and orbiting spacecraft like Kaguya (Yokota et al., 2009). Such an exo-ionosphere has also been modeled by Hartle and Killen (2006). While photo-ionization is considered the dominant exo-ionosphere source process, we investigate the possibility that the lunar ionosphere extends into nightside regions; this being driven by electron impact ionization (EII) processes associated nightside wake-energized electron populations.

To make the case, we apply new knowledge of surface secondary electron emission as recently discovered by Lunar Prospector (LP) (Halekas et al., 2009), our evolving understanding of the lunar plasma wake from LP and Kaguya (Halekas et al., 2005; Farrell et al., 2007; Nishino et al., 2009) and Apollo-era understanding of the thermally-driven surface helium concentration variations with lunation (Hodges, 1973; Stern, 1999). While electron impact ionization is a well-known process, we now tailor calculations to include our new understanding of the nightside terminator region including ambipolar-modified primary electrons and secondary electron beam emission in the formation of He^+ exo-ionosphere.

2. The He exosphere

Neutral helium is a dominant species in the lunar exosphere, with surface densities peaking at $4 \times 10^4/cm^3$ (Hodges, 1973). Arguably, only argon may be found in larger concentrations but its episodic release from the sub-surface suggests a larger temporal variability for this species (Stern, 1999). In contrast, the He exosphere is believed to form from quasi-constant re-emission of solar wind implanted He ions, making it ever-present in the near-surface environment.

Unlike argon, helium does not easily condense/adsorb onto the cold nightside surface Instead it maintains a neutral gas exospheric density in association with a $nT^{5/2}$ = constant relationship (Hodges and Johnson, 1968), T being the temperature of the accommodating lunar surface. As the surface temperature decreases, the He exosphere becomes increasingly dense. As such, the highest near-surface He concentrations are located in the coolest nightside regions. At dawn twilight, the rising surface temperature increases the gas scale height thus reducing the dayside concentration. Fig. 3 of Stern (1999) and Fig. 6 of Hodges (1973) shows the diurnal variation of near-surface neutral He as measured by the Lunar Atmosphere Composition Experiment (LACE). On the dayside, surface-level concentrations are below $2000/cm^3$ but in nightside regions are at levels of $\sim$40,000/cm^3. Table 1 lists nominal He concentrations in regions across the dusk terminator (having values slowly increasing with increasing SZA).

3. Nightside plasma environment

Spatially co-located over the He neutral gas volume is a solar wind plasma/lunar surface interaction region; this being an electrostatic interaction region creating a large-scale lunar wake, surface charging, and energetic electron populations. The region is illustrated in Fig. 1. Outward flowing plasma from the Sun, called the solar wind, is incident and (mostly) absorbed on the lunar dayside, creating a trailing plasma void or wake region (Ogilvie et al., 1996; Halekas et al., 2005). Generally, the plasma expands into this trailing void via ambipolar plasma processes: low mass electrons expand into the void along solar wind magnetic field lines ahead of the ions, creating a cross-wake E-field that then forces the ions inward (Crow et al., 1975; Samir et al., 1983; Ogilvie et al., 1996). As detected by LP at 20–155 km altitude (Halekas et al., 2005), the electron density of this primary solar wind component was found to exponentially decay for solar zenith angles (SZA) beyond 90° as shown in Fig. 1.

The nightside surface will achieve an equilibrium potential based on the current balance between electrons and ions that flow into the plasma void/wake region. This effect was modeled (Farrell et al., 2007) and the electron density (above the plasma sheath) and surface potential, $\phi_{surface}$, are both listed in Table 1. Note that the surface becomes increasingly negative beyond an SZA of 90° because the primary electrons reaching into the deeper regions of the nightside lunar surface have a steadily increasing temperature associated with energy-filtering of the tail of the solar wind kappa electron energy distribution (Halekas et al., 2005; Farrell et al.,

* Corresponding author at: NASA Goddard Space Flight Center, Code 695, Greenbelt, MD 20771, United States.
E-mail address: william.m.farrell@nasa.gov (W.M. Farrell).

0019-1035/$ - see front matter Published by Elsevier Inc.
doi:10.1016/j.icarus.2011.08.013

Table 1
The environmental parameters associated with electron impact ionization of helium near the lunar terminator. Rows 1–3 show the primary plasma electron density, temperature, and surface potential from the inflowing solar wind; this undergoing an ambipolar expansion into nightside regions (Farrell et al., 2007). Row 4 shows the surface helium density as measured by LACE (Hodges, 1973). Rows 6 and 7 are the primary and secondary chemical reaction rates derived using Eq. (5). Row 8 is the secondary electron density using Eq. (3). Finally, in the last row, the He ion production is quantified using the listed values in Eq. (4).

SZA	85°	90°	95°	100°	105°	110°	115°	120°
n_e (10^6/m^3)	2	1.4	0.8	0.5	0.2	0.14	0.09	0.06
T_e (eV)	12	14	17	20	23	28	31	34
Surface potential (V)	−10	−70	−90	−110	−132	−151	−185	−220
n_{He} (10^{10}/m^3)	1	1	2	2	2	2	3	3
k_p (10^{-15} m^3/s)	1.05	1.6	2.5	3.3	4.0	5.1	5.5	5.9
k_s (10^{-15} m^3/s)	0.0	17	27	34	35	35	36	37
n_s (1/m^3)	295,100	7400	3700	2100	750	610	300	163
He^+ production dn_{He+}/dt (1/m^3 s)	21.0	23.4	41.4	34.6	16.9	14.7	15.3	10.8

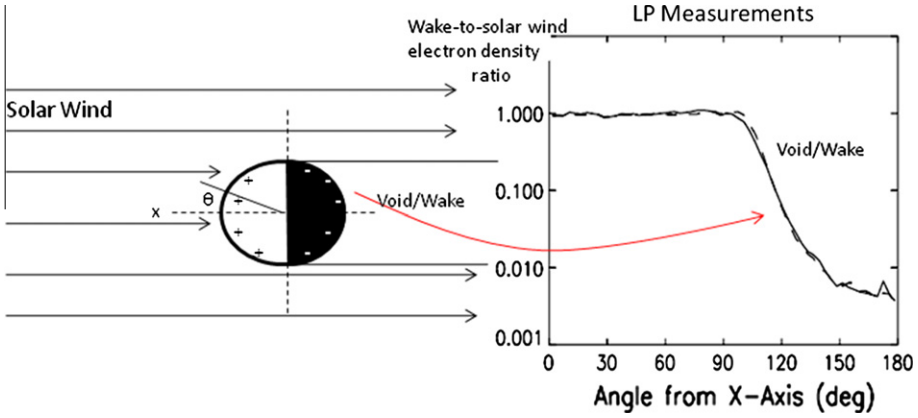

Fig. 1. Illustration of the lunar wake and corresponding Lunar Prospector electron density measurements of the void (from Halekas et al. (2005)).

2007). The kappa distribution is not isothermal but has a progressively increasing 'effective' temperature with energy. The effective temperature at a given energy can be defined as $-f(df/du)^{-1}$, where $f(u)$ is the electron energy distribution and u is the electron energy (in eV). For Maxwellian distributions, $-f(df/du)^{-1}$ is a constant. However, for kappa distributions, $-f(df/du)^{-1}$ progressively increases with increasing u. When passing into larger negative potentials, the resulting energy-filtered kappa electrons will thus appear warmer. The modeled electron temperature values (from Farrell et al. (2007)) are listed in Table 1.

Each of the filtered electrons that are incident at the lunar surface has a finite chance of releasing a secondary electron. This probability is a strong function of incident electron energy and impacted substrate. For lunar material, the secondary electron yield peaks near 300 eV at ~2.7 electrons released per incident electron. The overall yield drops below 1 electron released per incident electron at about 20 eV (see Horanyi et al. (1998) and references therein). Such secondary electrons are released from the surface at a few eV, but then are immediately accelerated outward along connecting magnetic field lines by the repulsive surface potential. They are then detected by low altitude spacecraft like LP and Kaguya in the form of a magnetic-field aligned quasi-monoenergetic electron beam (Halekas et al., 2007, 2009).

We want to obtain the He ionization rates that occurs at the top of the plasma Debye sheath, in a region just above where the secondary electrons have been accelerated by the surface potential, $\phi_{surface}$. The sheath geometry is illustrated in Fig. 2. Halekas et al. (2009) compared LP spacecraft observations of upward secondary electron fluxes, J_s, and incoming primary solar wind electron fluxes, J_e, and found they should vary at the surface as $J_s^{surface} \sim \eta J_e^{surface}$ with η near 0.8 (see their Fig. 3). For kappa distributions (with $\kappa \sim 4$), the primary electron current at the sheath top, J_e^{top}, is reduced by a factor of $J_e^{surface}/J_e^{top} \sim (1 + e|\phi_{surface}|/(2.5kT_e))^{-3}$ as it propagates to the negatively charged surface (Halekas et al., 2009). We can then express the approximate secondary electron concentration ejected by this sheath-altered primary current as

$$n_s^{surface} \sim \eta n_e^{top}(T_e/T_s)^{1/2}(1 + e|\phi_{surface}|/(2.5kT_e))^{-3} \quad (1)$$

where T_e/T_s is the ratio of the primary and secondary electron temperatures. These newly-ejected low-energy secondary electrons are then accelerated outward via the potential, $\phi_{surface}$, to the sheath topside region. For $e|\phi_{surface}| > kT_s$, the secondary electron density at this topside location is estimated to be

$$n_s^{top} \sim n_s^{surface}(kT_s/2\pi e\phi_{surface}|)^{1/2} \quad (2)$$

with $kT_{s/e} \sim 2$–3 eV (Manka, 1973) such that the topside flux of secondary electrons conserves momentum as it is accelerated outward by surface potential, $\phi_{surface}$. Combining Eqs. (1) and (2) provides the needed expression for the topside secondary electron density,

$$n_s^{top} \sim \eta(kT_e/2\pi e\phi_{surface}|)^{1/2} n_e^{top}(1 + e|\phi_{surface}|/(2.5kT_e))^{-3} \quad (3)$$

Table 1 lists the values of n_e^{top}, T_e, and $\phi_{surface}$ thereby allowing an easy quantification of n_s^{top}.

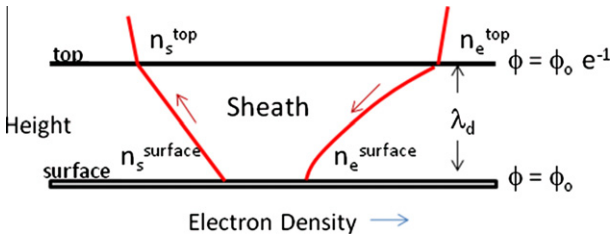

Fig. 2. The sheath geometry illustrating the primary and secondary electron density profiles.

4. The He reaction with energetic wake electrons

In the nightside terminator region, the neutral He gas and plasma electrons interact via the EII process. In a given volume of He, there are two interflowing electron components: One warm component with a broad energy distribution flowing towards the surface and an oppositely-directed quasi-monoenergetic electron beam at energy $e\phi_{surface}$, with beam energy determined by the surface potential at a location where the magnetic field line intercepts the surface. The Debye sheath size in the nightside region is estimated to be 10s of meters to a kilometers in size, while the scale height for the He is >100 km. As such, the surface density of the neutral He (Hodges, 1973) can be used as reasonable estimate at the topside of the sheath (and these concentrations are listed in Table 1). He ions produced by these two electron flows at the topside of the sheath can be expressed via

$$dn_{He+}/dt = k_p n_e^{top} n_{He} + k_s n_s^{top} n_{He} \quad (4)$$

where k_p and k_s are the chemical rates for electron impact ionization. In general, the rates k_p and k_s can be quantified by solving the integral (Ferreira,1983; Delory et al., 2006)

$$k_{p,s} = (2e/m)^{1/2} \int_{u_i}^{\infty} \sigma_{eii}(u)\, u f_{p,s}(u)\, du \quad (5)$$

where u is the electron energy, u_i is the He ionization energy, $\sigma_{eii}(u)$ is the He electron impact cross-section (Kieffer and Dunn, 1966) and $f_{p,s}(u)$ is the associated electron energy distribution for the primary and secondary electron component, respectively. The He EII cross-section is found to peak at ~135 eV with a value of $\sim 4 \times 10^{-21}$ m^2. The primary electron component is that expanding into the ambipolar region, and is in the form of a velocity-filtered kappa distribution containing only those electrons with energies, u, exceeding $e\phi_{ambipolar}$ at the observation point. In order to obtain an analytical solution to (5) we will approximate this filtered distribution with a Maxwellian distribution of the form $f_p(u) = 2\pi^{-1/2} u_e^{-3/2} \exp(-u/u_e)$, where $u_e = kT_e/e$, where T_e is the local electron temperature of the filtered electrons at the observation point. This local electron temperature is higher than that of the nominal solar wind electron temperature due to the higher effective temperature in the higher energy part of the distribution that passes through the potential filter (Farrell et al., 2007). The effect of this approximation is that we may slightly underestimate the values of k_p in our analysis in regions where the temperature-inflated Maxwellian distribution does not match the kappa distribution at $u \gg e\phi_{ambipolar}$. To obtain k_p, we thus solved Eq. (5) with $\sigma_{eii}(u)$ (Kieffer and Dunn, 1966) and $f_p(u, T_e(u = e\phi_{ambipolar}))$. The resulting values are listed in Table 1.

The quantification of k_s is easily derived assuming a quasi-monoenergetic secondary electron beam of the from $f_s(u) = u_b^{-1/2}\delta(u - u_b)$. In this case, $k_s = (2e/m)^{1/2}\sigma_{eii}(u_b)u_b^{1/2}$, with $u_b = |e\phi_{surface}|$. Values of $\phi_{surface}$ are also listed in Table 1.

Given the SZA profiles of the primary and secondary electrons, He density, surface potential, and chemical rates in Table 1, we can now solve Eq. (4) to derive the He ionization associated with EII. There are three immediate conclusions from this exercise: (1) The driving contribution to create the EII He^+ ionosphere are the primary, ambipolar-altered incoming electrons. However, secondary electron beams ejected from the surface do have a noticeable effect, creating additional ionization at 3–5% of the primary values at SZAs of 90–105°. The secondary electron beams near 100 eV are especially potent since they stimulate processes near the maximum EII cross-sectional values (Kieffer and Dunn, 1966). In regions where the surface potential is ~−100 V, an approximate estimate of the He^+ ion production is

$$dn_{He^+}/dt \sim 2.3 \times 10^{-15} (T_e/10\ \text{eV})^{1/2}\, n_e\, n_{He} \quad (6)$$

(2) As indicated in Table 1, electron impact ionization has its maximum effect near an SZA of 95–100° but continues to generate He^+ ions deeper into nightside regions. The peak in the EII activity is consistent with regions that have surface potentials near 100 eV. (3) Electron impact ionization nightside production of He^+ near the SZA of 100° is about 30% of that of dayside photo-ionization production at ~140/m^3 s (assuming a photo-ionization time of 162 days (Stern, 1999)). This finding does not suggest that EII is as efficient as the photo-ionization process. Instead, it reflects the large increase in He density from thermally-expanded dayside to compacted nightside configurations. (4) Besides the nightside He^+ component created by EII, there may also be times when the solar wind convection E-field drives photo-ionized dayside He^+ into the nightside region (Hartle and Thomas, 1974). Such flows would be expected at higher altitudes on the scale size of the lunar radius, suggesting the presence of two nightside He^+ layers: one near surface from local generation described herein and a second higher altitude flow from convectively-driven dayside photoions.

5. The currents of last resort and surface erosion

The new He^+ ions are born in the ambipolar region where the local E-field is directed primarily downward toward the surface. As such, these new ions represent a new environmental current component in the near-surface region. As described previously (Farrell et al., 2010), in the permanently shadow regions, the surface potential is defined by the balance of electron and ion currents that are capable of propagating through the ambipolar potential that forms along the wake flanks:

$$J_e^{ambipolar}(1 - \delta_s)\exp(e\phi_s/kT_e) + J_i^{ambipolar} = 0 \quad (7)$$

where $J_e^{ambipolar} = J_e^{sw}\exp(e\phi_{ambipolar}/kT_e)$, δ_s is the secondary electron coefficient (ejected from the surface), and $J_i^{ambipolar} \sim n_e^{sw}\exp(e\phi_{ambipolar}/kT_e)\, e\, ((\mathbf{v_{sw}}\text{-}\mathbf{v}_{ambipolar}).\mathbf{n})$. While the electrons are considered quasi-isotropic thermal flux, the solar wind ions have a directed flow at a specific angle relative to the surface normal, $\mathbf{n}$. The ambipolar E-field creates a deflection in the solar wind ion flow, pushing the ions beams effectively toward the surface. Thus local current balance at the surface (a solution for ϕ_s in Eq. (7)) exists as long as the dot product $(\mathbf{v_{sw}} - \mathbf{v_{ambipolar}}).\mathbf{n}$ is less than zero; in other words, at locations in a polar crater where the surface has direct access to the deflected solar wind ion flow.

However, with real topography, there are cases where the dot product $(\mathbf{v_{sw}} - \mathbf{v_{ambipolar}}).\mathbf{n}$ is greater than zero and the ion flow does not have direct incidence on the surface. Candidate locations for this effect are the leeward edges of polar/terminator craters that are immersed in an electron-rich plasma, called the 'electron cloud' (Crow et al., 1975; Farrell et al., 2010). Without the presence of solar wind ions, the surface would be expected to charge to anomalously large negative values until some other (as yet identified) remediation current forms to bring the system into current balance.

The downward directed current created by this local electron impact ionization of He^+ could be a possible remediation current that occurs in polar craters/obstructed solar wind flow to offset the loss of direct solar wind ion currents. Hence the new current balance in these strong negatively charged/electron cloud regions becomes

$$J_e^{ambipolar}(1 - \delta_s)\exp(e\phi_s/kT_e) + J_i^{EII}(\delta_s) + J^{DUST} = 0 \quad (8)$$

where locally-created downward EII ion currents and upward negatively-charged dust flux represented by J^{DUST} now replace the blocked flow from the filtered solar wind ion currents in defining current balance. In essence, if the solar wind-originating ion flow becomes obstructed, secondary processes in the local environment may create alternate downward-directed currents; such currents include local ionization of He^+ from the expanding plasma.

These effects should become especially intense within lunar polar craters. In these very cold regions, we can expect He to be very dense. As we demonstrated previously (Farrell et al., 2010), the lack of direct access to solar wind ions makes these crater floors charge to strongly negative values (below −100 V) and thus crater-trapped neutral He can be susceptible to the local primary and secondary (beam) electrons inflows into the region. Hence, in these craters, we may have the formation of a micro-ionosphere in association with the plasma expansion process. The downward-directed ambipolar E-field within the crater then immediately drives these new exo-ions right back into the surface, where they then behave as the needed ion current to complete the current balance process.

We note that this accelerated He^+ ion flux directed into the polar crater surface by the ambipolar and sheath fields is also a source of sputtering. For an accumulated ice layer within a polar crater (Spudis et al., 2010), the sputtering yield for ice being impacted by ~100 eV He^+ is nearly 1 molecule/ion (Johnson, 1990), making the water molecule loss rate comparable to the incoming He^+ flux. As such, these newly-borne He^+ ions can act as a high-mass sputtering source, even at relatively low energies.

While we assume the bulk of the argon exosphere is condensed onto the cold nightside surface and thus does not contribute to the nightside electron-driven ionosphere, it is recognized that there is an argon 'wind' at the sunrise terminator where desorbed species exposed to sunlight thermally-migrate back across the sunrise terminator into nightside regions (Stern, 1999). It is possible that a portion of this anti-sunward flow also becomes electron impact ionized, creating an Ar^+ component to the ionosphere. Also, Stubbs et al. (2011) recently suggested the presence of greatly enhanced electron concentrations at the terminator due to photo-electron emission from lofted dust, and the most energetic part of this population may also interact with the ambient He and Ar. There are thus other neutral-plasma processes to consider for future work.

To summarize, we demonstrate that the plasma-surface-neutral environment may be connected in new way; this coming to light with recent observations from LP and Kayguya. Specifically, lunar wake effects will create a tenuous but warm electron inflow to the nightside lunar surface, making the surface potential negative at a ~−100 V near SZA of 100–120°. The primary electron component along with surface-generated secondary electrons energized to ~100 eV are capable of ionizing the nightside cool, dense He neutral gas to form a near-surface He^+ exo-ionosphere. These interconnected plasma-surface-neutral processes could only be envisioned once there was a greater understanding of the lunar wake processes in combination with Apollo era understanding of the exosphere He. In the future, an ion spectrometer located on the surface (an updated suprathermal ion detector experiment (SIDE, see Collier et al., 2011)) and operating through terminator passages could confirm the presence of this electron-driven He^+ nightside ionospheres.

References

Collier, M.R. et al. (2011), Lunar surface electric potential changes associated with traversals of the terrestrial bow shock. Planet. Space Sci., in press.

Crow, J.E. et al., 1975. The expansion of plasma into a vacuum. J. Plasma Phys. 14, 65–76.

Delory, G.T. et al., 2006. Oxidant enhancement in martian dust devils and storms: Storm electric fields and electron dissociative attachment. Astrobiology 6, 451–462.

Farrell, W.M. et al., 2007. Complex electric fields near the lunar terminator: The near surface wake and accelerated dust. Geophys. Res. Lett. 34, L14201. doi:10.1029/2007GL029312.

Farrell, W.M. et al., 2010. Anticipated electrical environment within permanently shadowed lunar craters. J. Geophys. Res. 115, E03004. doi:10.1029/2009JE003464.

Ferreira, C.M., 1983. Current research topics in low-pressure glow discharges in rare gases and in pure nitrogen. In: Kunhardt, E.E., Luessen, L.H. (Eds.), Electrical Breakdown and Discharges in Gases. Part A: Fundamental Processes and Breakdown. Springer, New York, pp. 395–417.

Halekas, J.S. et al., 2005. Electrons and magnetic fields in the lunar plasma wake. J. Geophys. Res. 110, A07222. doi:10.1029/2004JA010991.

Halekas, J.S. et al., 2007. Extreme lunar surface charging during solar energetic particle events. Geophys. Res. Lett. 34, L02111. doi:10.1029/2006GL028517.
Halekas, J.S. et al., 2009. Lunar prospector measurements of secondary electron emission from lunar regolith. Planet. Space Sci. 57, 78–82.
Hartle, R.E., Killen, R., 2006. Measuring pickup ions to characterize the surfaces and exospheres of planetary bodies: Applications to the Moon. Geophys. Res. Lett. 33, L05201. doi:10.1029/2005GL024520.
Hartle, R.E., Thomas, G.E., 1974. Neutral and ion exosphere models for lunar hydrogen and helium. J. Geophys. Res. 79, 1519.
Hodges Jr., R.R., 1973. Helium and hydrogen in the lunar atmosphere. J. Geophys. Res. 78, 8055.
Hodges Jr., R.R., Johnson, F.S., 1968. Lateral transport in planetary exospheres. J. Geophys. Res. 73, 7307.
Horanyi, M. et al., 1998. Electrostatic charging properties of Apollo 17 lunar dust. J. Geophys. Res. 103, 8575.
Johnson, R.E., 1990. Energetic Charged Particle Interactions with Atmospheres and Surface. Springer-Verlag, Berlin.
Kieffer, I.J., Dunn, G.H., 1966. Electron impact ionization cross section data for atoms, atomic ions, and diatomic molecules: 1. Experimental data. Rev. Mod. Phys. 38, 1–35.
Manka, R.H., 1973. Plasma and potential at the lunar surface. In: Grard, R.J.L. (Ed.), Photon and Particle Interactions with Surfaces in Space. Reidel, Dordrecht, Netherlands, pp. 347–361.
Nishino, M.N. et al., 2009. Solar-wind proton access deep into the near-Moon wake. Geophys. Res. Lett. 36, L16103. doi:10.1029/2009GL039444.
Ogilvie, K.W. et al., 1996. Observations of the lunar plasma wake from the wind spacecraft on December 27, 1994. Geophys. Res. Lett. 23, 1255.
Samir, U. et al., 1983. The expansion of a plasma into a vacuum: Basin phenomena and processes and applications to space plasma physics. Rev. Geophys. 21, 1631–1646.
Spudis, P.D. et al., 2010. Initial results for the north pole of the Moon from Mini SAR, Chandrayaan 1 mission. Geophys. Res. Lett. 37, L06204. doi:10.1029/2009GL042259.
Stern, S.A., 1999. The Lunar atmosphere: History, status, current problems, and context. Rev. Geophys. 37, 455–491.
Stubbs, T.J. et al., 2011. On the role of dust in the lunar ionosphere. Planet. Space Sci., in press. doi:10.1016/j.pss.2011.05.011.
Yokota, S. et al., 2009. First direct detection of ions originating from the Moon by MAP-PACE IMA onboard SELENE (KAGUYA). Geophys. Res. Lett. 36, L11201.